L. Schippa & S. Pavan, Int. J. of Safety and Security Eng., Vol. 1, No. 4 (2011) 403–423

NUMERICAL MODELLING OF CATASTROPHIC EVENTS PRODUCED BY MUD OR DEBRIS FLOWS

L. SCHIPPA[1] & S. PAVAN[1]
[1]Department of Engineering, University of Ferrara, Italy.

ABSTRACT

Mud and debris flows are natural phenomena representing serious hazard for population and structures in mountain zones, because of their rapid occurrence and the difficulty in forecasting the phenomena initiation. Numerical models can however be useful in predicting the peak discharge and the strength of flowing mass, helping administrations in preparing risk mitigation measures. In this work, a numerical model for hyperconcentrated flows is presented. It is based on shallow water equations, with a particular source terms treatment which translates into an increased numerical stability and makes the model highly versatile. The test case applications focus on some fundamental characteristics necessary for debris- and mud-flow representation. In particular, classic dam-break problems have been used to test wave celerity and wet-dry fronts propagation, while a mud-flow dam-break problem has been chosen to investigate model sensibility to different rheological schemes. Then, the model has been applied to two real events that occurred in Northern Italy. The first one is a debris flow which took place at Acquabona, near Cortina d'Ampezzo. This event is extensively documented, since it has been observed by a monitoring station prepared by the University of Padua. The second one is a tragic event, during which the little town of Stava has been stricken by a destructive mud flow caused by the collapse of two earth dams.

Keywords: debris flow, mud flow, numerical simulation, source terms.

1 INTRODUCTION

Mud flow and *debris flow* are similar terms used to identify hyperconcentrated fluids, composed by a mixture of sediments and water, flowing over steep topography. The difference mainly lies in the sediment fine fraction, which is determinant for the fluid rheological behaviour [1, 2]. The use of the correct rheological scheme provides the basis for the reliable modelling of the phenomenon. Mud flows, characterised by high fine particles content, are well represented by yield-stress viscoplastic fluid models, among which the best known and widely used is the Bingham model [3]. On the other hand, granular debris flows dynamic can be described by granular fluid models such as the Bagnold model of inertial regime [4]. This is just a rough classification, deeper information can be found in the literature from the works of several authors [5–7]. However, even the most detailed classification is generally not sufficient to completely describe these kinds of events, since the sediment–water mixture is usually variable in time and space inside the same flow, and therefore the rheological behaviour is not homogeneous too.

One feature that surely is common to all hyperconcentrated flows is the destructive power. Though the dynamics of such fluids can be similar to that of water floods, their kinetic energy is up to one order of magnitude higher than that of clear water. This depends partially on the mixture density, which is almost double, and mainly on the flow velocity, which can be up to five times greater. The high destructive power translates into a risk which must be adequately defined and measured.

In general terms, two different points of view can be assumed when defining the acceptable risk level: the social point of view and the individual point of view [8]. Synthetically, the total risk associated with the different activities involving population can be assumed to be similar

ISSN: 2041-9031 (paper format), ISSN: 2041-904X (online), http://journals.witpress.com
DOI: 10.2495/SAFE-V1-N4-403-423

to what is accepted at an individual scale. In the specific situation of debris flows occurrence, the worst and less sustainable damages are related to buildings and road services destruction, since in both cases, the loss of human lives is frequent. In the first case, protection and debris diversion works are preferable for buildings protection, since the probability of people's presence inside buildings is very high. In the second case, the effective risk is related to the contemporary presence of people on the road, and therefore the risk can be assumed as acceptable if protection works are not present.

Nevertheless, the forecasting of sediment volumes moving and depositing over the interested areas during possible events, is fundamental in order to have reference scenarios and to evaluate the associated risk. The main task is therefore the prediction of flow parameters, among which the most important are the volume magnitude, the run-out distance, the momentum, and the impact force.

The aim of the present work is the setting-up of a numerical model suitable for the simulation of hyperconcentrated flows in channels of complex geometry. To fulfil this purpose, the model should have some specific features that will be examined in detail, such as the correct treatment of wet-dry fronts, the handling of complex geometries and steep bottom slopes, and the possibility of changing the model application field from Newtonian to non-Newtonian fluids, simply by changing the resistance law.

The proposed model is based on an alternative formulation of conservative balance equations, which includes a particular mathematical expression of source terms ideated for natural channels, and which has already demonstrated important stability features under the numerical point of view [9, 10]. This formulation is kept in the present work, while the innovation stands in the numerical implementation, since a finite volume method based on Roe's scheme is used instead of the MacCormack finite difference method [9, 10]. The main reason is the necessity of correctly capturing front wave propagation speed in case of initially dry bed, for which Riemann solvers-based techniques are recommended [11–14]. The second reason is the intention to verify if the model stability features are kept even if the numerical implementation radically changes.

Finite volume schemes are largely diffused in mud-flows treatment [15–18], and, among Riemann solvers, the Roe's approximation is often preferred [15, 17]. The presented model uses the same approach, paying careful attention in conserving a general formulation suitable for channels of complex geometry. This leads to a particular expression of the wave propagation celerity, which does not depend directly on water depth and cross-section width. For irregular cross-sections, these hydraulic parameters are often corrected or mediated to be representative. Alternatively, cross-section shape can be parameterised to be numerically handled with simplicity [18]. In order to avoid geometric simplifications or approximated parameters in this work, celerity is determined referring to the cross-section wetted area and static moment. This ensures the formulation generality.

For what concerns the source terms treatment, one should distinguish between pressure terms and friction terms. The pressure source terms, induced by the channel irregular geometry have been treated mathematically transforming the longitudinal derivative of the static moment in order to eliminate the explicit dependence from the channel bed slope [9, 10]. Friction source term mainly depends on the rheological behaviour of the mixture. Like most of numerical models [19], the proposed model setup permits to easily change the resistance law and therefore to use the best fitting rheological model for each test case. Finally, source term numerical implementation has been kept as simple as possible, to put in evidence the stability features coming from the basic mathematical model. Source terms are therefore computed with the Euler's method and handled using the splitting technique [11].

All the mentioned features have been investigated choosing specific test cases. The classic frictionless dam-break test has been used to verify the correctness of waves speed propagation and the capability of treating wet-dry fronts. A non-prismatic frictionless ideal channel has been used to evaluate the model response to abrupt changes in cross-sections width and bed elevation. Then, the effect of friction terms addition has been checked using a mud-flow dam-break, for which the analytical solution is available. This test permits to consider and compare different resistance formulas, and can also be used as a testing ground for the introduction of different rheological schemes inside the model. It is also useful for testing the wave front propagation speed and the liquid–solid discharge stopping conditions. The model has been further tested using laboratory experiments on mud-flow dam-break over a sloping plane. Finally, it has been applied to two real events that occurred in Northern-Eastern Italy. The first one is a debris flow which took place in 1998 in the Upper Valley of River Boite, near Cortina d'Ampezzo. The second one is a mud flow event that occurred in the Stava Creek Valley in 1985.

2 MATHEMATICAL MODEL

The model is based on shallow water equations, written in conservative form for one-dimensional flows in natural channels of complex geometry. We assume a one-phase model. State variables are the wetted cross-section area A and the discharge Q [12, 20].

$$\frac{\partial A}{\partial t}+\frac{\partial Q}{\partial x}=q \tag{1}$$

$$\frac{\partial Q}{\partial t}+\frac{\partial}{\partial x}\left(\frac{Q^2}{A}+gI_1\cos\vartheta\right)=gA\left(S_0-S_f\right)+gI_2\cos\vartheta \tag{2}$$

where t is time, x is the distance along the channel, q is the lateral inflow per channel unit length, α is the Coriolis coefficient (for the sake of simplicity it is herein assumed to be equal to unity), g is the gravitational acceleration, ϑ is the angle between the bottom line and the horizontal, I_1 is the static moment of the wetted area, I_2 is the variation of I_1 along the x-direction, S_0 is the bottom slope, and S_f is the friction slope.

$$I_1=\int_0^{h(x)} b\left(x,z\right)\left(h\left(x\right)-z\right)\,\mathrm{d}z \tag{3}$$

$$I_2=\left.\frac{\partial I_1}{\partial x}\right|_h \tag{4}$$

$$S_0=\sin\vartheta=-\frac{\partial z_b}{\partial x} \tag{5}$$

where z is the vertical coordinate, $b(x,z)$ is the local cross-section width, $h(x)$ is the local water depth, and $z_b(x)$ is the bottom elevation.

The resistance formula approach deals with the shear stress formulation, which in turn depends on the rheological model. Generally speaking, the friction term can be computed according to three different schemes: (a) one-phase model, accounting for the overall resistance behaviour of the solid–fluid mixture; (b) two-phase model, considering separately the contribution to the resistance force associated with liquid and solid phases; (c) multi-layer model, assuming a number of superimposed flowing layers, each one with a specific flow resistance

behaviour. An appreciable review of these models can be found, as an example, in [13], whereas significant information about two-phase models can be found in [15].

In the present model, a lumped rheological model is assumed. As a consequence, the hyperconcentrated flow is treated as a continuum, and the basic shear stress is adopted inside the depth-averaged momentum equation:

$$S_f = \frac{\tau}{\rho g R} \tag{6}$$

where R is the hydraulic radius, defined as A/P (P being the wetted perimeter), ρ is the mixture density, and τ is the shear stress.

Let us consider the longitudinal derivative of the static moment of the wetted area I_1:

$$\frac{\partial I_1}{\partial x} = \frac{\partial}{\partial x}\int_0^{h(x)} b(x,z)\big(h(x)-z\big)\mathrm{d}z \tag{7}$$

by applying the Leibniz integral rule, we obtain:

$$\frac{\partial I_1}{\partial x} = \int_0^{h(x)} \frac{\partial}{\partial x}\Big[b(x,z)\big(h(x)-z\big)\Big]\mathrm{d}z + b(x,z)\big(h(x)-h(x)\big) \tag{8}$$

$$\frac{\partial I_1}{\partial x} = \int_0^{h(x)} \frac{\partial}{\partial x}\Big[b(x,z)\big(h(x)-z\big)\Big]\mathrm{d}z \tag{9}$$

Accounting for the product rule:

$$\frac{\partial I_1}{\partial x} = \int_0^{h(x)} \left[b(x,z)\frac{\partial\big(h(x)-z\big)}{\partial x} + \big(h(x)-z\big)\frac{\partial b(x,z)}{\partial x}\right]\mathrm{d}z \tag{10}$$

where z is the local vertical coordinate and does not depend on x, therefore $\partial z/\partial x = 0$ and

$$\frac{\partial I_1}{\partial x} = \frac{\partial h(x)}{\partial x}\int_0^{h(x)} b(x,z)\mathrm{d}z + \int_0^{h(x)} \big(h(x)-z\big)\frac{\partial b(x,z)}{\partial x}\mathrm{d}z \tag{11}$$

Accounting for the definition of the wetted area and of I_2, the longitudinal derivative of the static moment I_1 results as the sum:

$$\frac{\partial I_1}{\partial x} = \frac{\partial h(x)}{\partial x}A + I_2 \tag{12}$$

On the other hand, the reference plane (datum), from which the water surface elevation z_w is measured, is completely arbitrary, and can be assumed to be equal to local channel bottom elevation z_0. In this way, we have:

$$I_1 = I_1(h,x) = I_1(z_w,x) \tag{13}$$

and therefore the derivative of the static moment is:

$$\frac{\partial I_1}{\partial x} = \frac{\partial I_1}{\partial z_w}\frac{\partial z_w}{\partial x} + \left.\frac{\partial I_1}{\partial x}\right|_{z_w} \tag{14}$$

Accounting for the definition of water depth, we have:

$$\frac{\partial h}{\partial x} = \frac{\partial \left(z_w - z_0 \right)}{\partial x} = \frac{\partial z_w}{\partial x} + S_0 \tag{15}$$

Combining eqns (12), (14), and (15), we obtain:

$$A\frac{\partial z_w}{\partial x} + AS_0 + I_2 = \frac{\partial I_1}{\partial z_w}\frac{\partial z_w}{\partial x} + \left.\frac{\partial I_1}{\partial x}\right|_{z_w} \tag{16}$$

Since:

$$\frac{\partial I_1}{\partial z_w} = \frac{\partial I_1}{\partial h} = A \tag{17}$$

we finally obtain:

$$I_2 = \left.\frac{\partial I_1}{\partial x}\right|_{z_w} - AS_0 \tag{18}$$

The substitution of eqn (18) inside eqn (2) brings to:

$$\frac{\partial Q}{\partial t} + \frac{\partial}{\partial x}\left(\frac{Q^2}{A} + gI_1 \cos\vartheta \right) = gA\left(S_0 - S_f \right) + \left.\frac{\partial I_1}{\partial x}\right|_{z_w} \cos\vartheta - AS_0 \cos\vartheta \tag{19}$$

or

$$\frac{\partial Q}{\partial t} + \frac{\partial}{\partial x}\left(\frac{Q^2}{A} + gI_1 \cos\vartheta \right) = gAS_0\left(1 - \cos\vartheta \right) + gAS_f + g\left.\frac{\partial I_1}{\partial x}\right|_{z_w} \cos\vartheta \tag{20}$$

Considering the momentum balance eqn (20), it is worth noting the presence of the "reduced bottom slope" $S_0(1 - \cos\vartheta)$. Nevertheless, comparing the reduced bottom slope $S_0(1 - \cos\vartheta)$ with the friction slope S_f, it is clear that the latter has a different order of magnitude if compared with the former. This is true in particular in case of ϑ less than 30°, being $\cos\vartheta > 0.87$. Therefore, for the sake of simplicity we assume $gAS_0(1 - \cos\vartheta) + gAS_f \approx gAS_f$ and $\cos\vartheta \approx 1$.

3 NUMERICAL MODEL

Shallow water equations have been numerically implemented using the first-order finite volumes Godunov scheme. Numerical fluxes are computed with Roe's method and source terms are evaluated with Euler's approach and taken into account adopting the splitting technique. Details on the different components of the numerical model can be found in [11]. The resultant scheme is explicit, first-order accurate, and has a very uncomplicated structure, since it is built choosing the simplest solution technique for every component of the partial differential equations system. This approach has the intention to illustrate the intrinsic stability features of the mathematical model, which could otherwise be hidden by more sophisticated numerical schemes.

In order to write the shallow water equation in a compact form, three vectors can be introduced:

$$\mathbf{U} = \begin{pmatrix} A \\ Q \end{pmatrix} \tag{21}$$

U is the vector representing the system unknowns, varying in time, which are in fact the state variables of balance equations.

$$\mathbf{F} = \begin{pmatrix} Q \\ \dfrac{Q^2}{A} + gI_1 \end{pmatrix} \tag{22}$$

F is the fluxes vector, representing the hydraulic quantities stored inside each cell. The flux terms vary along the *x* coordinate, and their variation expresses the mass and pressure exchanges between adjacent cells.

$$\mathbf{S} = \begin{pmatrix} q \\ g\dfrac{\partial I_1}{\partial x}\bigg|_{z_w} - gAS_f \end{pmatrix} \tag{23}$$

S is the source terms vector, accounting for side mass addition, channel shape variation, and flow resistance, that are the main external driving forces for fluid motion.

Indicating with the subscript *t* and *x* the derivatives with respect to time and space, the entire equations system is summarised as:

$$\mathbf{U}_t + \mathbf{F}(\mathbf{U})_x = \mathbf{S}(\mathbf{U}) \tag{24}$$

Referring to this compact formulation, the splitting approach for the treatment of source terms consists in separately solving the homogeneous partial differential equation system (25) and then the ordinary differential eqn (26), adopting the solution of eqn (25) as initial condition.

$$\mathbf{U}_t + \mathbf{F}(\mathbf{U})_x = 0 \quad \Rightarrow \quad \bar{\mathbf{U}} \tag{25}$$

$$\mathbf{U}_t = \mathbf{S}(\bar{\mathbf{U}}) \quad \Rightarrow \quad \mathbf{U}_{\mathrm{t+dt}} \tag{26}$$

The solution of eqn (25) is found applying a Godunov type scheme, in which numerical fluxes **F** are computed by means of the Riemann problem solution between adjacent cells. Considering the borderline between cells *i* and *i*+1, and assigning to it the position *x* = 0, the *local Riemann problem* is an initial value problem posed as:

$$\begin{cases} \mathbf{U}_t + \mathbf{F}(\mathbf{U})_x = 0 \\ \mathbf{U}(x,t^n) = \begin{cases} \mathbf{U}_i^n & x < 0 \\ \mathbf{U}_{i+1}^n & x > 0 \end{cases} \end{cases} \tag{27}$$

One of the most used numerical methods to solve the Riemann problem is the Roe's approximation, which linearises the initial system of conservation laws by means of a coefficient matrix which substitutes the fluxes vector:

$$\mathbf{U}_t + \mathbf{J}(\mathbf{U})\mathbf{U}_x = 0 \tag{28}$$

Therefore, the Roe's scheme requires the definition of the so-called Jacobian matrix:

$$\mathbf{J} = \frac{\partial \mathbf{F}}{\partial \mathbf{U}} = \begin{pmatrix} 0 & 1 \\ g\dfrac{\partial I_1}{\partial A} - \dfrac{Q^2}{A^2} & 2\dfrac{Q}{A} \end{pmatrix} = \begin{pmatrix} 0 & 1 \\ c^2 - u^2 & 2u \end{pmatrix} \tag{29}$$

In particular, the Roe's approach consists in defining a constant coefficient matrix, based on the Riemann initial value problem for every computational cell:

$$\mathbf{J} = \mathbf{J}(\mathbf{U}_i, \mathbf{U}_{i+1}) \tag{30}$$

Most of models proposed in the literature, which include the solution of shallow water equations for debris flow or for natural channels, by means of approximate Riemann solvers, adopt the same simplification in the evaluation of the term $\partial I_1/\partial A$ [15, 21], assuming

$$\frac{\partial I_1}{\partial A} \cong \frac{A}{B} \cong h \quad \Rightarrow \quad c = \sqrt{g\frac{A}{b}} \quad or \quad c = \sqrt{gh} \tag{31}$$

Similarly, in Zanuttigh and Lamberti [18], a prismatic channel configuration has been assumed, in order to simplify the source term inside balance equations, and get a more stable behaviour of the numerical model.

In the present model, in order to keep the formulation generality and to ensure the applicability to natural and complex channel geometries, the static moment derivative is explicitly computed as the ratio between the variations of I_1 and A, considering a water depth variation range $h \pm \Delta h$ close to the actual water depth h:

$$\frac{\partial I_1}{\partial A} = \frac{I_1(h+\Delta h) - I_1(h-\Delta h)}{A(h+\Delta h) - A(h-\Delta h)} \tag{32}$$

The celerity c is therefore defined as:

$$c = \sqrt{g\frac{\partial I_1}{\partial A}} \tag{33}$$

The new equations system (28) is still an hyperbolic system, it will therefore have m real eigenvalues $\lambda_j(\mathbf{U}_i, \mathbf{U}_{i+1})$ and m real eigenvectors $K(\mathbf{U}_i, \mathbf{U}_{i+1})$, with $m = 2$ when considering one-dimensional flow. It is possible to project the initial problem vectors $\mathbf{U}_i$ and $\mathbf{U}_{i+1}$ along these eigenvectors by means of the *wave strength coefficients* α_j.

$$\Delta\mathbf{U} = \mathbf{U}_{i+1} - \mathbf{U}_i = \sum_{j=1}^{m} \alpha_j K^j \tag{34}$$

The Roe's numerical flux can finally be expressed in three equivalent ways:

$$\mathbf{F}_{i+1/2} = \mathbf{F}_i + \sum_{\lambda j<0} \lambda_j \alpha_j K^j \tag{35}$$

$$\mathbf{F}_{i+1/2} = \mathbf{F}_{i+\frac{1}{2}} + \sum_{\lambda j>=0} \lambda_j \alpha_j K^j \tag{36}$$

$$\mathbf{F}_{i+1/2} = \frac{1}{2}(\mathbf{F}_i + \mathbf{F}_{i+\frac{1}{2}}) - \frac{1}{2}\sum_{j=1}^{m} |\lambda_j| \alpha_j K^j \tag{37}$$

The expressions for eigenvectors, eigenvalues, and *wave strengths* are:

$$K_j = \begin{bmatrix} 1 \\ \tilde{u} \pm \tilde{c} \end{bmatrix} \tag{38}$$

$$\lambda_j = \tilde{u} \pm \tilde{c} \tag{39}$$

$$\alpha_1 = \frac{(c+u)\Delta A - \Delta Q}{2c} \; ; \; \alpha_2 = \frac{(c-u)\Delta A + \Delta Q}{2c} \tag{40}$$

In which:

$$\tilde{u} = \frac{Q_{i+\frac{1}{2}}\sqrt{A_i b_i} + Q_i \sqrt{A_{i+\frac{1}{2}} b_{i+\frac{1}{2}}}}{\sqrt{A_i A_{i+\frac{1}{2}}}\left(\sqrt{A_i b_{i+\frac{1}{2}}} + \sqrt{A_{i+\frac{1}{2}} b_i}\right)} \tag{41}$$

$$\tilde{c} = \sqrt{\frac{g}{2}\left(\left.\frac{dI_1}{dA}\right|_i + \left.\frac{dI_1}{dA}\right|_{i+\frac{1}{2}}\right)} \tag{42}$$

Another important aspect of Godunov finite volume method application to natural geometries is the quantification of cells water volume V and the definition of the relation between the state variable A and V. For every computational cell, A is defined as:

$$A_i = \frac{1}{\Delta x}\int_{x_{i-\frac{1}{2}}}^{x_{i+\frac{1}{2}}} A(x,t)\,\mathrm{d}x = \frac{V_i}{\Delta x} \tag{43}$$

Referring to Fig. 1, V_i is computed as the volume of a truncated pyramid, where bases are irregular polygons, since the water profile is assumed to be parallel to channel bed.

$$V_i = \frac{\left(A_{i-\frac{1}{2}} + A_{i+\frac{1}{2}} + \sqrt{A_{i-\frac{1}{2}} A_{i+\frac{1}{2}}}\right)\Delta x}{3} \tag{44}$$

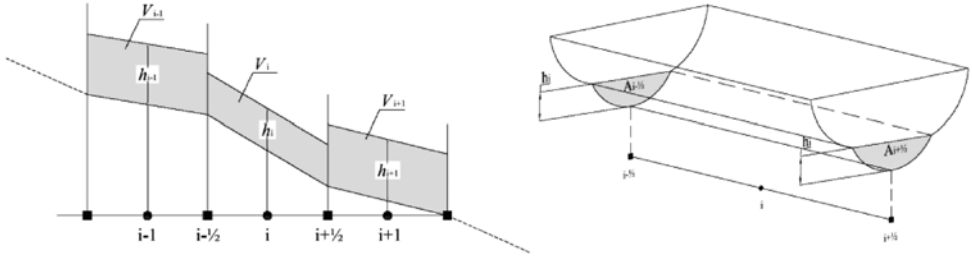

Figure 1: Computational scheme for V_i.

4 SOURCE TERMS NUMERICAL TREATMENT

Source terms are numerically included in computations by splitting, and they are simply computed by Euler's method considering no lateral inflows.

$$\mathbf{U}_{\mathrm{t+dt}} = \mathbf{U}_t + \Delta t \cdot \mathbf{S}\left(t, \bar{\mathbf{U}}\right) \tag{45}$$

in which

$$\mathbf{S} = \begin{pmatrix} 0 \\ g\left.\dfrac{\partial I_1}{\partial x}\right|_{z_w} - gAS_f \end{pmatrix} \tag{46}$$

The momentum balance source term is composed of two parts: the friction term and the pressure term. The latter is represented by the static moment variation along channel, taking the water surface elevation as a constant.

This particular formulation requires the assumption of a horizontal water surface with a constant water level in every computational cell, differently from the parallel water profile configuration assumed for the solution of the homogenous system.

The constant value of z_w is obtained by finding the horizontal water elevation which gives the same cell fluid volume as that computed by eqn (44).

The computational scheme for the pressure term quantification in represented in Fig. 2, and the variation of I_1 is computed as:

$$\left.\frac{\partial I_1}{\partial x}\right|_{z_w} = \left.\frac{\Delta I_1}{\Delta x}\right|_{z_w} = \frac{I_1\left(h_{i+\frac{1}{2}}\right) - I_1\left(h_{i-\frac{1}{2}}\right)}{\Delta x} \tag{47}$$

Adopting this computational scheme, particular situations can arise when water depth is small and bottom slope is high, as it happens for example to cell *i* in Fig. 2. In this case, in fact, the term $I_1(h_{i-1/2})$ is equal to zero. This problem is overcome by reducing the cell length Δx proportionally to the wet cell portion.

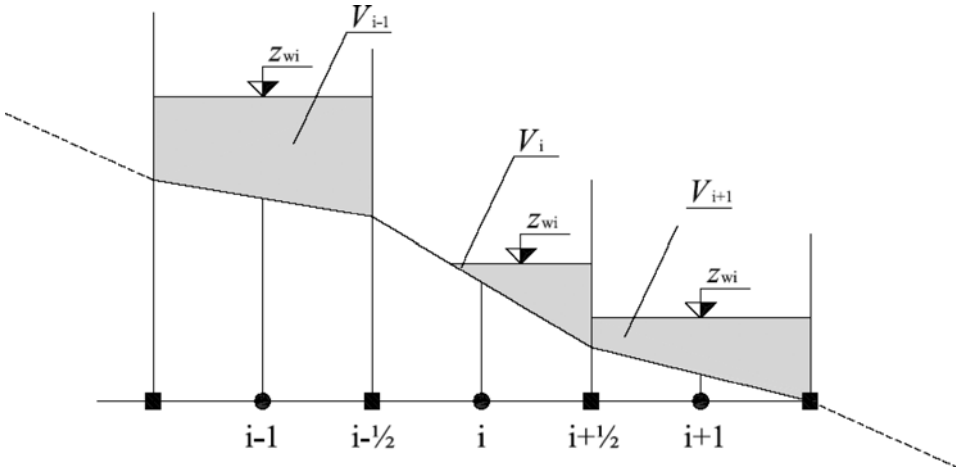

Figure 2: Computational scheme for momentum balance pressure source term.

5 NUMERICAL TESTS

Five test cases have been selected to investigate the performances of the proposed mathematical model and numerical scheme. Test cases 1 and 2 are idealised problems of dam-break in a rectangular channel with dry bed and wet bed, respectively. These examples have been chosen in order to check the model capability to address wet-dry fronts and to compute the correct wave speed propagation. The third test case proposes the simulation of water at rest inside a non-cylindrical frictionless idealised channel, and is used to check the model response to geometrical and pressure source terms. With test case 4 the attention is shifted to non-Newtonian fluids, with a mud-flow dam-break over horizontal bed. In this test case, the aim is to verify the correctness of the rheological model and the role of friction source terms. Finally, test case 5 refers to laboratory experiments about mud-flow dam-break over a sloping plane.

After the testing phase, the model has been applied to two real events. The first one is a natural debris flow event, due to intense rainfall, surveyed at the Acquabona site in Northern Italy. It is of particular interest thanks to the large amount of available field data. The second is the Stava mud flow, a tragic episode occurred in a little town of Italian Alps. This event was caused by the collapse of two tailing dams, which released a huge quantity of water into the Stava Creek channel, causing the formation of a mud flow wave with an enormous destructive power.

6 IDEALISED DAM-BREAK PROBLEM IN A RECTANGULAR CHANNEL WITH DRY BED

Let us consider a 10 m long rectangular channel, with horizontal and frictionless bed. A dam is located in the middle, 5 m far from upstream and downstream ends. Water depth upstream the dam is 1.5 m, while downstream the bed is dry. In the simulations, $\Delta x = 0.1$ m is set, while Δt is determined by the Courant–Friedrichs–Lewy stability condition assuming a CFL number equal to 0.9.

In Fig. 3a, the comparison between analytical and numerical solution is shown at time $t =$ 0.7 s. The classical Ritter's solution can be found in Toro [11]. Wave front velocity is slightly underestimated, but it is coherent with the adopted numerical scheme. The use of the partial derivative of the static moment I_1 with respect to wetted area A in the definition of the celerity

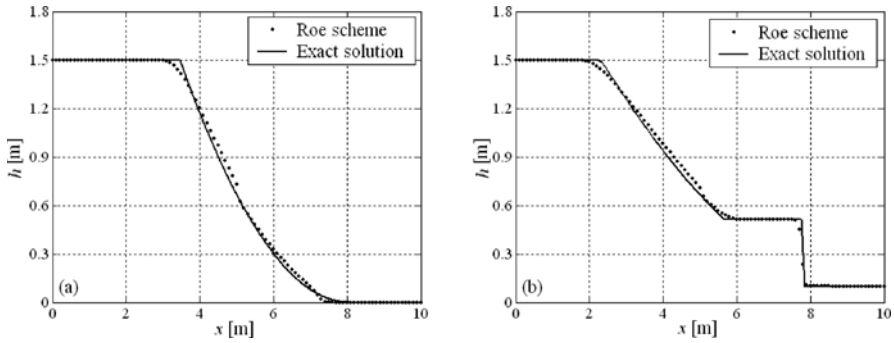

Figure 3: Comparison between analytical and numerical solution for the dam-break problem over dry bed (a) and over wet bed (b).

(eqn (33)), instead of the water depth h, does not affect the efficiency of the numerical scheme. The water profile discontinuity at $x = 5$ m is related to the need of an *entropy fix* correction for the Roe's approximated Riemann solver. In this case, the Harten–Hyman *entropy fix* has been used.

7 IDEALISED DAM-BREAK PROBLEM IN A RECTANGULAR CHANNEL WITH WET BED

The channel geometry is same as the previous test case, but the downstream water depth is set at 0.1 m. In this case, the element to check is the propagation velocity of the downstream shock wave. The analytical solution can be found in Stoker [22]. In Fig 3b, the comparison between analytical and numerical solution is shown at time $t = 0.4$ s. The essential features of the flow, such as front location, shock wave height, and front speed are well captured. As it is expected from the adopted first-order scheme, a slight diffusivity is present at solution discontinuity points. As in the previous case, the Harten–Hyman *entropy fix* correction has been added to reduce water profile discontinuity at $x = 5$ m.

8 NON-CYLINDRICAL RECTANGULAR CHANNEL TEST

This test case, proposed by Goutal and Maurel [23], presents a hypothetical frictionless channel, in which width and bottom elevation vary discontinuously along the longitudinal profile. Every cross-section is rectangular in shape. As shown in Fig. 4a and b, this test presents abrupt bottom slope variations and sudden bank narrowing or widening, in particular at station $x = 800$ m, channel breadth changes rapidly from 40 to 5 m. The geometry is completely described by 29 cross-sections, the total length is 1500 m, and it has been divided into 1500 computational cells, assuming a constant cell dimension of 1 m. The simulated flow condition is water at rest. Null discharge is imposed upstream ($Q_M = 0$ m^3/s) and a constant level $z_{wV} = 12$ m is kept downstream, as boundary conditions. The initial condition is still water with constant level $z_{w0} = 12$ m and zero discharge $Q_0 = 0$ m^3/s at every cross-section. Computation has been performed accounting for the Courant–Friedrichs–Lewy stability condition, using a Courant number equal to 0.85.

The same test case has been treated by the authors in a previous work [9] in which the proposed mathematical model has been implemented with the McCormack numerical scheme, obtaining for both discharge and water surface elevation with a computational

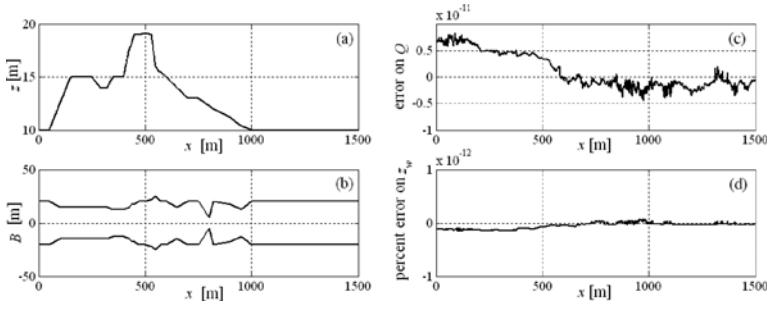

Figure 4: Non-cylindrical rectangular channel test: bed profile (a), channel plan (b), and numerical simulation errors on Q (c) and on z_w (d).

precision of 10^{-14}. The application of the first-order Roe's scheme leads to computational errors around 10^{-11}, but it can be considered as a satisfactory result if compared with the results of Garcia-Navarro and Vazquez-Cendon [21] model on the same test case. In their work, the Roe's approximate solver and the finite volume numerical scheme were applied in association with another source terms treatment. The comparison with the results reported in Garcia-Navarro and Vazquez-Cendon [21] highlights the role of the proposed mathematical treatment of pressure source terms.

9 MUD-FLOW DAM-BREAK ON A HORIZONTAL BED

The fourth test case has the double function to shift the attention from Newtonian to non-Newtonian fluids and to verify the insertion of friction source terms inside the numerical model. To this end, the Hungr [24] test case has been selected. Hungr gives a solution for a plastic fluid based on an approximated energy solution for a dam-break problem on a horizontal bed 1500 m long, with the dam positioned at x = 305 m far from upstream. The initial water depth upstream the dam is 30.5 m, while downstream the bed is dry. The stopping location for the water–solid mixture is expected to be at x = 1896 m, under Hungr's assumption for yield stress and density. This test is usually employed to compare different flow resistance relations, since it furnishes an analytical reference solution [19]. In this work, three rheological models have been implemented and inserted into the model. The formulations and used parameters are summarised in Table 1.

For the numerical simulations the cannel has been divided into 1500 cells of constant width. Results are shown in Fig. 5. Except for slight differences in the final flow profile, the analytical stopping position is satisfactorily approached. The aim of this test case, however, is not the specific verification of different rheological models, but of the general model response to their implementation. This aim can therefore be considered as fulfilled. Another important confirmation is the model flexibility, since various flow resistance relationships can be indifferently used. In further testing, there will be the possibility of choosing the best fitting rheological model.

Table 1: Flow resistance relations and parameters.

Resistance law	Formulation	Parameters
Full Bingham	$S_f = \frac{\tau_0}{\rho g h}$ with τ_0 from: $2\tau_0^{\,3} - 3\left(\tau_y + 2\frac{\mu_B q}{h^2}\right)\tau_0^{\,2} + \tau_y^{\,3} = 0$	μ_B = 100 Pa·s, τ_y = 1500 N/m^2, ρ = 1835 kg/m^3
Simplified Bingham	$S_f = \frac{\tau_0}{\rho g h}$ with: $\tau_0 = 1.5\tau_y + 3\frac{\mu_B q}{h^2}$	μ_B = 100 Pa·s, τ_y = 1500 N/m^2, ρ = 1835 kg/m^3
Turbulent, Coulomb, & Yield	$Sf = \frac{n^2 q\sqrt{q^2}}{h^2 h_r^{4/3}} + \frac{\tau_i}{\rho g h}$ with: $\tau_i = \min\left(\tau_y; \rho g h \cos\vartheta \tan\delta\right)$	n = 0.0667 s/m$^{1/3}$, δ = 10°, τ_y = 500 N/m^2, ρ = 1835 kg/m^3

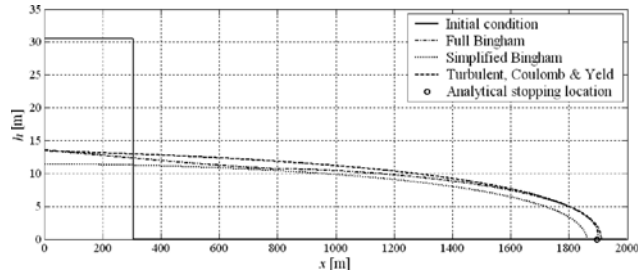

Figure 5: Mud-flow dam-break results for different resistance formulae.

10 MUD-FLOW DAM-BREAK ON A SLOPING PLANE

In this test case, numerical results are compared with the experimental results of Laigle and Coussot [17]. The experimental device consisted of a 4 m long and 0.6 m wide flume, in which a sluice, positioned at 0.85 m from the upstream end was rapidly pulled up reproducing a quasi-instantaneous dam-break for the solid–liquid mixture. Flow depths were measured by three ultrasonic gauges positioned at 1.65, 2.75, and 3.85 m far from the upstream end, during the experiments. Several tests have been performed changing the plane slope from 6% to 31%. During the simulated experiment, the flume had a 16% slope. The mixture had a measured density $\rho = 1410$ kg/m^3 and yield stress $\tau_y = 19$ Pa. The rheological model adopted is the same proposed by Laigle and Coussot [17] in their work. Mixture behaviour can in fact be described by the Herschel–Bulkley model, which, for simple shear conditions, can be written as:

$$\tau = \tau_c + K\gamma^{\eta} \tag{48}$$

where K and η are rheological parameters. In the selected experiment, K results to be 3.5 Pa·s$^{1/3}$, while η has been empirically set equal to 1/3. Numerical and experimental results are compared in terms of peak height h_P, residual height h_R, and front arrival time t_F in Table 2, while Fig. 6 shows the mixture profile development at different time steps (a) and the computed hydrographs corresponding to the three measuring gauges (b). In general, peak height is slightly underestimated, while the residual height is sensibly overestimated for gauge 3. The wave front shows a little delay for gauges 1 and 3, while it is just in time at gauge 2. However, measured hydrographs are generally correctly captured for what concerns their shape, dimension, and position in time.

11 ACQUABONA DEBRIS FLOW

The Acquabona debris flow has been widely surveyed and documented in the context of the Debris Flow Risk project of the European Commission (ENV4-CT96-0253). In particular, the research concentrated on some debris flow-prone watersheds in the Upper Boite Valley (Eastern Dolomites, Southern Alps) near the municipality of Cortina d'Ampezzo [25]. A large quantity of field data is therefore available since an automatic, remotely controlled monitoring system has been installed at Acquabona in June 1997. The Acquabona site is characterised by one or more debris flow every year, which usually occur in summer and in early autumn and are associated with intense but spatially limited rainfall events. Acquabona debris flow, although classified as hill-slope-type, according to the definition by Brunsden [26] and Costa [27], is currently deeply channelised in the scree, and its flow path is well defined. This results in high risk for the national road and the factories in the valley bottom.

Table 2: Comparison between experimental and numerical results for the mud-flow dam-break experiments by Laigle and Coussot.

Variable	Experimental	Computed
Gauge 1		
t_F (s)	0.48	0.58
h_P (cm)	2.56	2.53
h_R (cm)	1.06	0.97
Gauge 2		
t_F (s)	1.38	1.38
h_P (cm)	2.12	2.08
h_R (cm)	0.94	0.97
Gauge 3		
t_F (s)	2.13	2.24
h_P (cm)	1.87	1.73
h_R (cm)	0.69	0.92

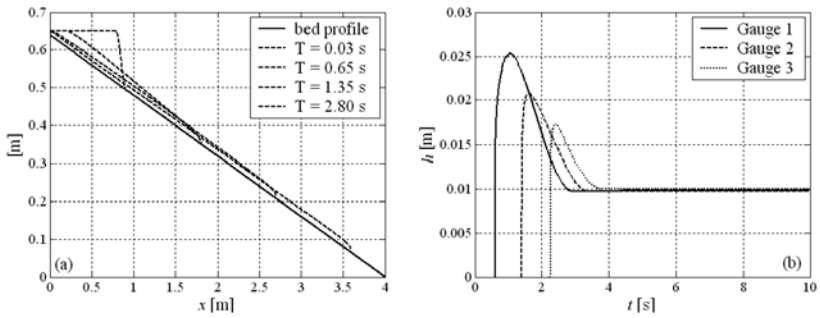

Figure 6: Mud-flow dam-break experiments by Laigle and Coussot: (a) mixture profile evolution in time; (b) flow depth vs time at three measuring gauges.

The upper drainage basin of Acquabona is characterised by dolomite rocks and by a deep channel cut in heterogeneous deposits. The steep rock basin is almost entirely made up of moderately fractured dolomite, but is not affected by karst phenomena. It has an effective drainage area of 0.30 km^2, average slope of 38°, and maximum length of only 1300 m. These characteristics translate into a rapid hydrological response to intense rainfall: collected water quickly reaches the outlet of the basin and meets a narrow rocky channel, full of debris. If rainfall intensity is sufficiently high, the flow may exceed the relatively limited drainage capacity of the channel bed material and surface flow occurs. The whole process starts 30–45 minutes after the peak intensity of precipitation and ends in the following 20–40 minutes, indicating a rapid hydrological response of the system in which the contribution of groundwater flow is negligible. The monitoring system installed at Acquabona was fully automatic and remotely controlled. It consisted of three on-site monitoring stations and an off-site

master collection station. Every station was equipped with a geophone, and at Station 3 a superficial pressure transducer and an ultrasonic sensor was present too.

In this work, we refer to the event that occurred on 17 August 1998. The event was originated by a very intense rainstorm: 25.4 mm of rain were measured in 30 minutes by the rain gage at Station 1. The volume of the deposits available for debris flow generation has been estimated to be around 8000–9000 m^3. The overall duration of the event was of approximately 38 minutes and more than 20 different surges have been surveyed at Station 3.

The geometry of the channel is available thanks to 19 surveyed transversal cross-sections. The global channel length is 1120 m and the altitude difference is 245 m. The longitudinal slope ranges from 10% to 55%. For model application, a constant spatial step of 1 m has been adopted. Numerical simulations were performed using the rainfall hydrograph reconstructed by Orlandini and Lamberti [28], which covers a period of about 2.5 hours and presents a peak discharge of 2.3 m^3/s. An open-type boundary condition is imposed at the downstream end. For the debris flow the bulk concentration is assumed to be equal to 0.6 and the mixture density equal to 1850 kg/m^3, according to Zanuttigh and Lamberti [18].

The Acquabona debris flow transports gravely sandy poorly sorted material, ranging in size from silt and clay to big boulders (up to 1–2 m in diameter). The material is essentially cohesionless. The rheological model adopted for simulations is the Herschel–Bulkley model (eqn (48)). Referring to the simulations carried out by Fraccarollo and Papa [16] on the same event, K is assumed to be 150 $Pa \cdot s^{1/3}$, τ_c is equal to 925 N/m^2, and η has been empirically set equal to 1/3.

In Fig. 7, the computed flow height is compared with measured data collected by the ultrasonic sensor at Station 3. The model satisfactorily captures height and shape of the waves, but it underestimates their duration, overestimating as a consequence, their number. Results are, however, encouraging and comparable with those obtained by Fraccarollo and Papa [16] and Zanuttigh and Lamberti [18].

The average velocity of the different flow surges has been estimated through geophones log recordings, which have been used to identify the instants of surges' transition on each surveying station. Available data refer to two 100 m long channel reaches located in the lower part of the channel, before and after Station 3 (which corresponds to the surveyed cross-section 8). Comparison is shown in Fig. 8. In the upstream reach, computed velocities compare well with field data, while in the downstream reach they are generally overestimated.

It is interesting to note that the flow regime is mainly characterised by the formation of roll waves, as it is evident by observing the longitudinal distribution of discharges and flow depths at two subsequent time steps (Fig. 9). Nevertheless, numerical solution is not affected by relevant numerical instabilities.

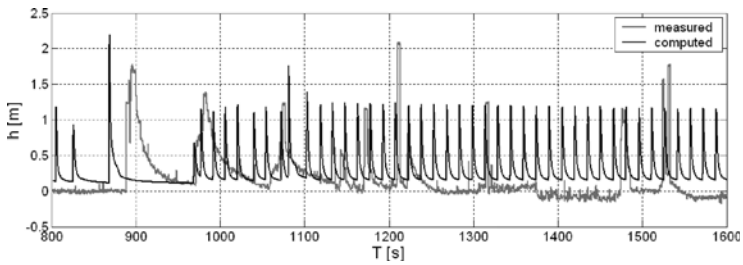

Figure 7: Comparison between the flow depth measured and calculated at Station 3.

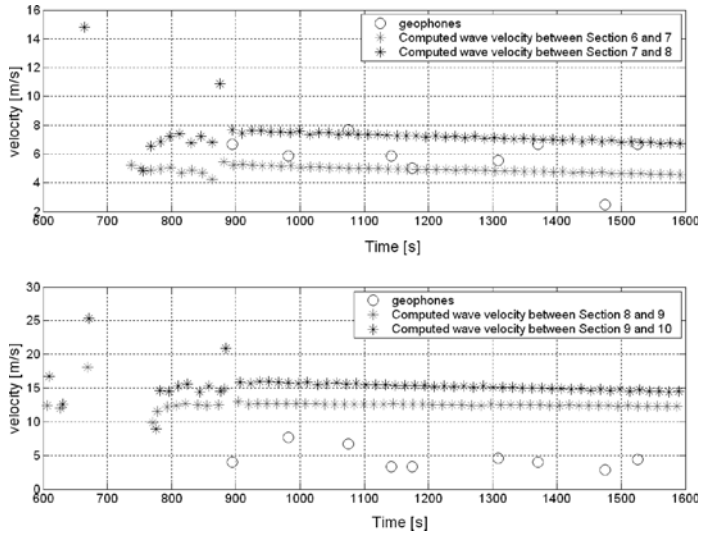

Figure 8: Comparison between measured and computed wave speed upstream and downstream Station 3.

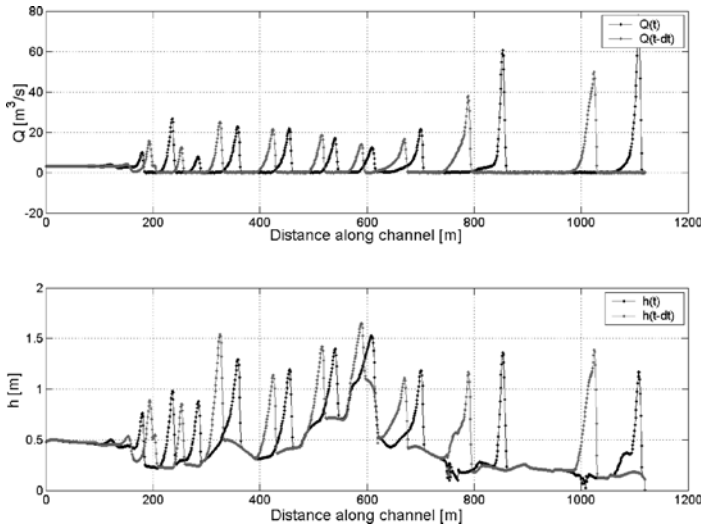

Figure 9: Longitudinal discharge distribution and flow depth profile.

It is important to point out that a physically based numerical model, once rheological parameters have been accurately chosen and calibrated using one or more significant events, could be used as a prediction tool for the same kind of phenomena in neighbouring mountain basins, characterised by a similar orography and debris composition.

Debris flow prediction remains however a challenging task, because of the rapid flow triggering and of the mass flow velocity. A real-time alert system would therefore require a rapid response both from the local civil protection system and from the population itself. A more

effective way of using numerical prediction model results would be to recognise and delimit risk-prone areas by identifying the debris run-out length.

12 STAVA MUD FLOW

On 19 July 1985, two tailing dams suddenly collapsed at Tesero, a little town in the Italian Alps, near Bolzano. The stored water, together with the dam body material, flowed down to the Stava River as a big mud flow, claiming 268 human lives and destroying 47 houses. As reported by Takahashi [4], the Stava River before the disaster flowed with an approximately uniform slope of 5°. Although the mud flow had such an intensive destructive power, as well as fluidity, the Stava River channel itself had not suffered much erosion or deposition, and it can therefore be simulated as a fixed bed stream. Probably, no erosion occurred because the solid fraction inside the water–sediment mixture was so high (estimated to be about 0.48) that the flow could not easily become denser by erosion.

In his report, Takahashi gave important references about particles size, which was so fine that the relative depth, R/d, was about 10^5. In this condition, the resistance to flow is similar to that of a plain water flow and the Manning's equation can be applied. Takahashi obtained a Manning's roughness coefficient in each section by reverse calculation from the data on velocity computed with the Lenau's formula applied to measure flow superelevations at bends.

The channel description is taken from Takahashi [5] too. It includes 24 surveyed cross-sections, their plan location, and the longitudinal profile. In this case, bed slope ranges from 5% to 12%. The simulated reach is 3500 m long and a constant spatial step of 1.25 m has been used. A longitudinal variability in the flow cross-section shape is noticeable: beyond the natural unevenness, a decreasing tendency of channel width is recognisable in the downstream direction between Station 4 and Station 10, then the cross-section abruptly increases in the proximity of Station 10 and 10′, then it keeps approximately constant downstream.

In Fig. 10, discharge and depth computed hydrographs are compared with Takahashi's numerical results obtained with the kinematic wave theory [5]. Referring to cross-section 10, located about 3000 m downstream the dams, there is a good accordance between the computed

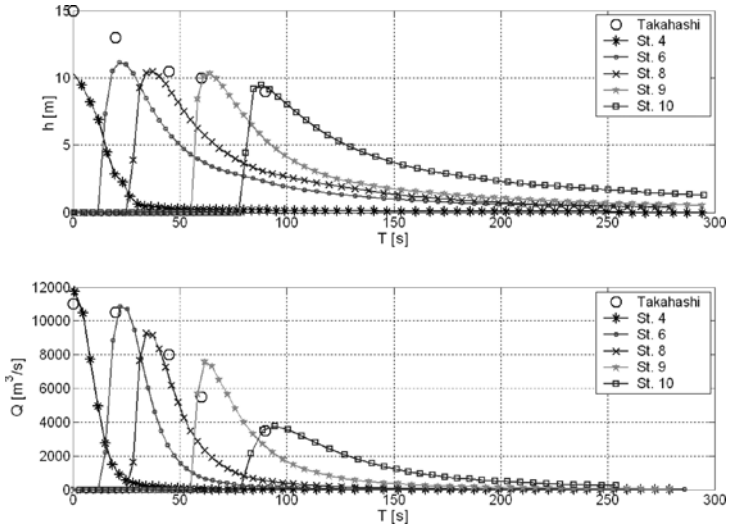

Figure 10: Depth and discharge hydrograph at different cross-sections.

peak discharge and the value estimated by Takahashi (3500 m^3/s), as the result of the product between the wetted cross-section area is measured *in situ* (about 500 m^2) and the maximum velocity is derived by the flow superelevation at the nearest bend (7 m/s). Attenuation of peak water elevation and discharge in such an abrupt flow of short duration is considerable.

The correct estimation of peak discharge and water depth, together with mass front velocity, are among most important parameters to identify when protection structures are planned.

The initial water profile condition reproduces the same hypothesis adopted by Takahashi, that is, a uniform slide of the mud mass until Section 4, from which the mud flow is assumed to develop. The initial condition and further development of the flow surface profile are shown in Fig. 11.

Figure 12 shows the comparison between computed and measured front arrival instants at different distances along the channel. The measured values are estimated on the basis of a seismograph located at Cavalese, a nearby town. The computed times are in good agreement with the estimated ones along the entire channel.

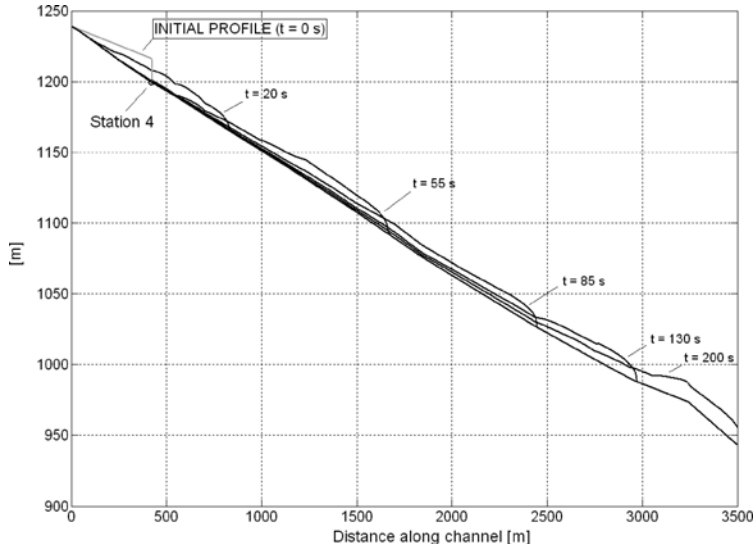

Figure 11: Initial conditions and flow profiles along the channel during the simulation.

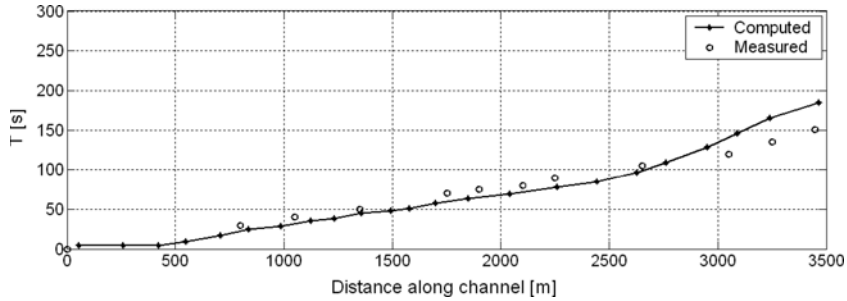

Figure 12: Comparison between computed and measured front arrival times at different locations.

13 CONCLUSIONS

A numerical model useful in predicting mud flow and debris flow natural events is presented. It is based on a mathematical model, in which main features are concerned with the propagation of the wet-dry fronts, the treatment of irregular and variable cross-sections shape, and the applicability to steep channels. Different test cases have been selected in order to verify these features. The classic frictionless dam-break test has been used to test the correctness of waves speed propagation and the capability of treating wet-dry fronts. The source terms treatment has been verified independently, analysing the influence of pressure terms with a non-prismatic frictionless idealised channel, while the role of friction terms has been tested with a mud-flow dam-break, for which the analytical solution is available. This test has been performed using different resistance laws, and also permitted to check model flexibility for what concerns the adopted rheological model. Eventually, the model has been tested using laboratory experiments on mud-flow dam-break over a sloping plane. Numerical results compare favourably with experiments in terms of front wave speed, peak height, and residual front thickness. After this first phase of model validation, in which all the fundamental features have been investigated and ascertained, two real events have been chosen to finally test the model. The first one is a natural debris flow event that occurred at Acquabona. In this case, a large quantity of field data was available, allowing the comparison with simulation outputs. Model results compared well with wave peak height and propagation velocities. The second test case refers to the Stava mud flow tragic event, originated by the collapse of two tailing dams. Good accordance between observed data and measured mud flow front propagation speed has been obtained. Simulation results have been also compared with the Takahashi's analysis of the same event, showing good accordance for what concerns the evaluation of peak discharge at different cross-sections.

The model represents a useful tool in forecasting hyperconcentrated flows. It leads to the prediction of flow parameters, among which the most important are the volume magnitude, the run-out distance, the momentum, and the impact force (derived from the flow hydrographs).

The presented model performs satisfactorily in natural irregular streams. The source term rearrangement avoids any problem in modelling adverse or very steep slopes, since the pressure term is evaluated for a constant water surface elevation. The lumped rheological model seems particularly suitable for representing a large variety of hyperconcentrated flows.

REFERENCES

[1] Julien, P.Y. & Lan Y.Q., Rheology of hyperconcentrations. *Journal of Hydraulic Engineering*, **117(3)**, pp. 346–353, 1991. doi:http://dx.doi.org/10.1061/(ASCE)0733-9429(1991)117:3(346)

[2] Johnson, A.M., *Physical Processes in Geology*, W.H. Freeman: San Francisco, Calif., 1970.

[3] Chen, C.L., Generalized viscoplastic modelling of debris flow. *Journal of Hydraulic Research, ASCE*, **114(3)**, 1988.

[4] Takahashi, T., *Debris flow, IAHR Monograph Series*, A.A. Balkema: Rotterdam Brookfield, p. 165, 1991.

[5] Iverson, R.M., Hydraulic modelling of unsteady debris-flow surges with solid-fluid interaction. *Debris Flow Hazards Mitigation: Mechanics, Prediction and Assessment*, ASCE, New York, NY, 1997.

[6] Rickenmann, D. & Koch, T., Comparison of debris flow modelling approaches. *Debris Flow Hazards Mitigation: Mechanics, Prediction and Assessment*, ASCE, New York, NY, 1997.
[7] Takahashi, T., Debris flow on prismatic open channel. *Journal of the Hydraulics Division*, **106(HY3)**, pp. 381–396, 1980.
[8] Vrijling, J.K., Hengel, W. & Houben, R.J., A framework of risk evaluation. *Journal of hazardous materials*, **43**, pp. 245–261, 1995. doi:http://dx.doi.org/10.1016/0304-3894(95)91197-V
[9] Schippa, L. & Pavan, S., Analytical treatment of source terms for complex channel geometry. *Journal of Hydraulic Research*, **46(6)**, pp. 753–763, 2008.
[10] Schippa, L. & Pavan, S., Bed evolution numerical model for rapidly varying flow in natural streams. *Computer & Geosciences*, **35**, pp. 390–402, 2009. doi:http://dx.doi.org/10.1016/j.cageo.2008.08.004
[11] Toro, E.F., *Riemann Solvers and Numerical Method for Fluid Dynamics*, Springer-Verlag: Berlin Heidelberg New York, 1999.
[12] Cunge, J.A., Holly, F.M. & Verswey, A., Practical aspects of computational river hydraulics, *The Pitman Advanced Publishing Program*, 1980.
[13] Hutter, K., Svendsen, B. & Rickenmann, D., Debris-flow modelling: a review. *Continuum Mechanics and Termodynamics*, **8**, pp. 1–35, 1996. doi:http://dx.doi.org/10.1007/BF01175749
[14] Ying, X. & Wang, S.S.Y., Improved implementation of the HLL approximate Riemann solver for one-dimensional open channel flows. *Journal of Hydraulic Research*, **46(1)**, pp. 21–34, 2008. doi:http://dx.doi.org/10.1080/00221686.2008.9521840
[15] Brufau, P., Garcia-Navarro, P., Ghilardi, P., Natale, L. & Savi, F., 1D Mathematical modelling of debris flow. *Journal of Hydraulic Research*, **38(6)**, pp. 435–446, 2000. doi:http://dx.doi.org/10.1080/00221680009498297
[16] Fraccarollo, L. & Papa, M., Numerical simulation of real debris-flow events. *Physics and Chemistry of the Earth*, **25(9)**, pp. 757–763, 2000. doi:http://dx.doi.org/10.1016/S1464-1909(00)00098-8
[17] Laigle, D. & Coussot, P., Numerical modelling of mudflows. *Journal of Hydraulic Engineering*, **123(7)**, pp. 617–623, 1997. doi:http://dx.doi.org/10.1061/(ASCE)0733-9429(1997)123:7(617)
[18] Zanuttigh, B. & Lamberti, A., Analysis of debris wave development with one-dimensional shallow-water equations. *Journal of Hydraulic Engineering*, **130(4)**, pp. 293–303, 2004. doi:http://dx.doi.org/10.1061/(ASCE)0733-9429(2004)130:4(293)
[19] Naef, D., Rickenmann, D., Rutschmann, P. & McArdell, B.W., Comparison of flow resistance relations for debris flow using a one-dimensional finite element simulation model. *Natural Hazards and Earth System Sciences*, **6**, pp.155–165, 2006. doi:http://dx.doi.org/10.5194/nhess-6-155-2006
[20] Mambretti, S., Larcan, E. & De Wrachien, D., 1D modelling of dam-beak surges with floating debris. *Biosystems Engineering*, **100**, pp. 297–308, 2008. doi:http://dx.doi.org/10.1016/j.biosystemseng.2008.02.011
[21] Garcia-Navarro, P. & Vazquez-Cendon, M.E., On numerical treatment of the source terms in the shallow water equations. *Computer & Fluids*, **29**, pp. 951–979, 2000. doi:http://dx.doi.org/10.1016/S0045-7930(99)00038-9
[22] Stoker, J.J., Water waves. *The Mathematacal Theory with Applications*. John Wiley and Sons, Toronto, Canada, 1992.

[23] Goutal, N. & Maurel, F., *Proceedings of the 2nd workshop on dam-break wave simulation*, Direction des études et recherches, Electricité de France, Rep. HE43/97/016/B, 1997.

[24] Hungr, O., A model for the run-out analysis of rapid flow slides, debris flow, and avalanches. *Canadian Geothecnical Journal*, **32(4)**, pp. 610–623, 1995. doi:http://dx.doi.org/10.1139/t95-063

[25] Berti, M., Geneovis, R., Simoni, A. & Tecca, P.R., Field observations of a debris flow event in the Dolomites. *Geomorphology*, **29**, pp. 265–274, 1999. doi:http://dx.doi.org/10.1016/S0169-555X(99)00018-5

[26] C. Embleton & J. Thornes, Brunsden, D., Mass movements. *Process and geomorphology*, ed. E. Arnold, London, pp. 131–186, 1979.

[27] Costa, J.E. & Williams, G.P., *Debris flow dynamics, Film, Open File Report 84/606*. U.S. Geological Survey, Water Resources Division: USA, 1984.

[28] Orlandini, S. & Lamberti, A., Effect of wind precipitation intercepted by steep mountain slopes. *Journal of the hydrologic engineering*, **5(4)**, pp. 346–354, 2000. doi:http://dx.doi.org/10.1061/(ASCE)1084-0699(2000)5:4(346)